Journal of Materials Chemistry C

Accepted Manuscript

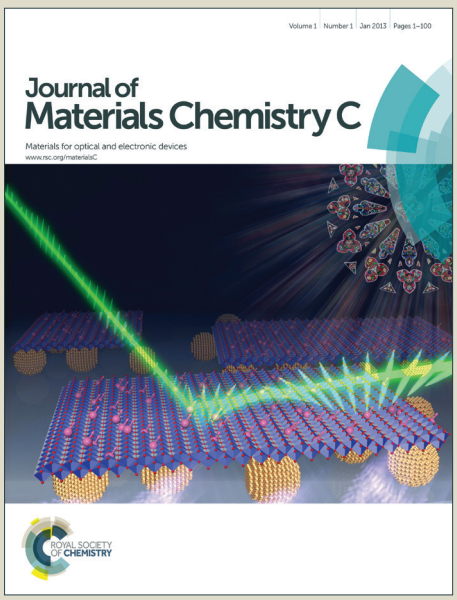

ROYAL SOCIETY OF CHEMISTRY

www.rsc.org/materialsC

Highly Twisted Biphenyl-Linked Carbazole-Benzimidazole Hybrid Bipolar Host Materials for Efficient PhOLEDs

Shuo-Hsien Cheng,[a] Wen-Yi Hung,*[b] Ming-Hung Cheng,[b] Hsiao-Fan Chen,[a] Atul Chaskar,[a] Gene-Hsiang Lee,[a] Shu-Hua Chou,[a] Ken-Tsung Wong*[a,c]

[a] *Department of Chemistry, National Taiwan University, Taipei, 10617, Taiwan.*

[b] *Institute of Optoelectronic Sciences, National Taiwan Ocean University, Keelung, 20224, Taiwan.*

[c] *Institute of Atomic and Molecular Sciences, Academia Sinica, Taipei, 10617, Taiwan.*

Graphic abstract

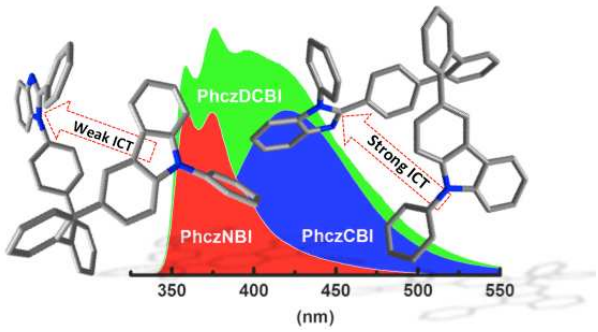

Three highly twisted bipolar molecules with different degree of charge transfer characters are developed to serve as PhOLEDs host materials.

Abstract

Three new highly twisted bipolar host materials (**PhczNBI**, **PhczCBI,** and **PhczDCBI**) comprising of a biphenyl core linking a hole-transport 9-phenylcarbazole (donor) and an electron-transport *N*-phenylbenzimidazole (acceptor) with different topology were synthesized, characterized, and applied as host materials for full-color phosphorescent OLEDs. The highly twisted conformations imparted through a 2,2'-biphenyl linkage effectively disrupt the π-conjugation and electronic coupling between the donor and the acceptor, thus, giving the bipolar hosts promising properties such as bipolar charge transport features ($\mu_h \approx \mu_e \approx 10^{-6}$–$10^{-4}$ $cm^2V^{-1}s^{-1}$) and high triplet energies (E_T = 2.55–2.71 eV). The PhOLED device gave a maximum external quantum efficiency (η_{ext}) of 19.6% for **PhczNBI** host with a yellow phosphor $(Bt)_2Ir(acac)$. A two-color, single-emitting-layer and all-phosphor WOLED hosted by **PhczDCBI** achieved high efficiencies (13.9%, 34.9 cd A^{-1}, and 24.8 lm W^{-1}) and a CRI up to 65.5.

Introduction

Phosphorescent OLEDs (PhOLEDs) have been deemed as the most potential candidates to realize full-colour flat-panel display and solid state lighting applications due to their intrinsic capability of harnessing both singlet and triplet excitons through effective intersystem crossing (ISC).[1,2] Therefore, PhOLED devices can achieve nearly 100% internal quantum efficiency by utilizing heavy metal-centred complexes as emitters.[3] To suppress the detrimental effects such as aggregation quenching and/or triplet-triplet annihilation, which often are the main issues to deteriorate the device efficiency[4], host–guest strategy with triplet emitters (guest) homogeneously dispersed into a suitable organic matrix (host) is frequently used. Therefore, the design of appropriate host materials is of great importance for highly efficient PhOLEDs and should meet the following criteria: (i) sufficient high triplet energy (E_T) for assuring exothermic energy transfer from the host material to the dopant and efficient exciton confinement,[5] (ii) suitable energy level match-ups with adjacent layers to reduce interfacial energy barriers and to increase charge balance,[6] (iii) high and balanced bipolar transport capability to well define charge recombination zone within the emissive layer, and (iv) high morphological stability.[7] Among them, the demands of high E_T and good bipolar transport capability are generally conflicting for organic molecules because the introduction of electron-donating (D) and -withdrawing (A) moieties easily triggers intramolecular charge transfer character that lowers the energy gap and thus a lower E_T. As a result, an efficient way to minimize electronic coupling between D and A is always required for the design of high E_T bipolar hosts.

Various strategies have been developed to achieve bipolar hosts with high E_T by impeding electronic communication between D and A. For example, the introduction of saturated bridging centre such as C or Si atom between D and A

segments can efficiently interrupt the through-bond electronic communication and confine the π-conjugation within individual component.[8-12] For example, Yang and Ma *et al.* recently reported new-type bipolar host materials in which a Si atom was introduced to bridge an arylamino donor and benzimidazole or oxadiazole acceptors. These materials were shown to possess high E_T in a range of 2.69–2.73 eV.[9,10] Interestingly, these new host materials were found to be capable of serving as universal hosts for blue, green and orange phosphors to give their corresponding devices with external quantum efficiency (η_{ext}) as high as 16.1%, 22.7%, and 20.5%, respectively. Besides, fluorene has also been adopted as an effective non-conjugated spacer through its sp^3-hybridized C9 atom.[11] Our previous research also demonstrated the successful utilization of fluorene as an effective non-conjugated bridge for D and A at the C9- and C3-positions, respectively.[12] The E_T for this series of bipolar hosts can be as high as 2.86 eV, rendering remarkable η_{ext} of 15.1%, 17.9%, and 20% for blue, green, and red PhOLEDs, respectively. Another strategy to reduce electronic coupling between D and A is to incorporate a linker with highly twisted conformation to minimize effective π-conjugation. It can be achieved by introducing multiple *ortho*-connections between D and A to impart severe steric hindrances, which largely twist the molecule into non-coplanar manners. Such twisted molecular conformation is also beneficial to the formation of amorphous thin films with enhanced morphological stability because of less accessible π-planes for the formation of intermolecular π-stacking. For instance, Ma and Yang *et al.* recently reported a series of highly twisted bipolar hosts based on carbazole-phosphine oxide hybrid and a 2,2'-biphenyl bridge. The twisted conformation renders an E_T as high as 3.01 eV, which is suitable for hosting blue phosphors. A maximum η_{ext} of 19.5% was achieved for deep blue PhOLEDs.[13]

In this work, we adopted the advantages of the highly twisted molecular

conformation to design three new bipolar host materials, **PhczNBI**, **PhczCBI**, and **PhczDCBI** by introducing proper D and A moieties onto the 2,2'-positions of a biphenyl linker. Hole-transport carbazole and electron-transport benzimidazole[14] have been judiciously selected as the D and A moieties, respectively, due to their excellent carrier transport properties and high E_T. The regioisomeric **PhczNBI** and **PhczCBI** were designed with different linking topology (*N*- and *C*-connectivity of the benzimidazole, respectively) to explore their structure-property-performance relationship with different effective conjugation and E_T. Our previous studies have shown that the *N*-connected isomers possessed higher E_T than those of their *C*-connected analogues.[15] Moreover, the analogous **PhczDCBI** was designed based on direct connectivity of the benzimidazole to the biphenyl linker without the phenyl spacer. **PhczDCBI** is expected to possess a higher E_T which may lead to much efficient blue PhOLED devices. We investigated the thermal, photophysical, electrochemical, and carrier-transport properties of these three host materials with respect to their molecular structures. Blue, green, yellow, and white phosphorescent OLEDs were fabricated based on **PhczNBI**, **PhczCBI**, and **PhczDCBI**. Among them, **PhczDCBI** revealed the exceptionally high device efficiencies with low efficiency roll-off with η_{ext} of 12.3%, 15.1%, 16.1%, and 13.9% for blue, green, yellow, and white PhOLED devices, respectively. **PhczNBI**-hosted yellow PhOLED also exhibited a remarkable η_{ext} of 19.6%. These results strongly suggested a successful molecular design strategy of bipolar hosts for highly efficient PhOLEDs.

Results and Discussion

Synthesis

Scheme 1 shows the synthetic pathways and structures of the highly twisted

bipolar hosts, **PhczCBI**, **PhczNBI**, and **PhczDCBI**. The precursor 2-bromo-2′-iodobiphenyl (**1**) was prepared in 67% yield *via* aryl-aryl coupling based on corresponding organolithium reagents according to the literature.[16] Then, *N*-phenylcarbazole was introduced by selective Suzuki-Miyaura cross-coupling of **1** and *N*-phenylcarbazole-3-boronic ester (**2**) to afford **3** in 70% yield. Both **PhczCBI** and **PhczNBI** were synthesized in 62% yields by Suzuki-Miyaura cross-coupling of **3** and *N*-biphenylbenzimidazole boronic esters, **4** and **5**, respectively. **PhczDCBI** was synthesized by Suzuki-Miyaura cross coupling of the boronic ester intermediate (**7**) and 2-(2-bromophenyl)-1-phenyl-1*H*-benzimidazole (**8**) in 73% yield, in which **7** was obtained in overall 76% yield by successive Suzuki-Miyaura cross-coupling starting from **2** and 1-bromo-2-iodobenzene. Detailed synthetic procedures and the characterization data are summarized in the Electronic Supplementary Information (See ESI in detail).

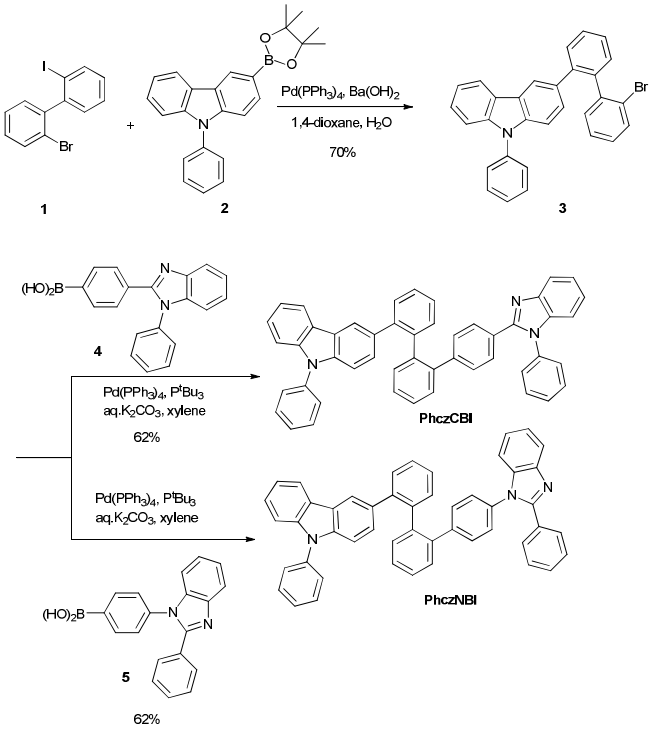

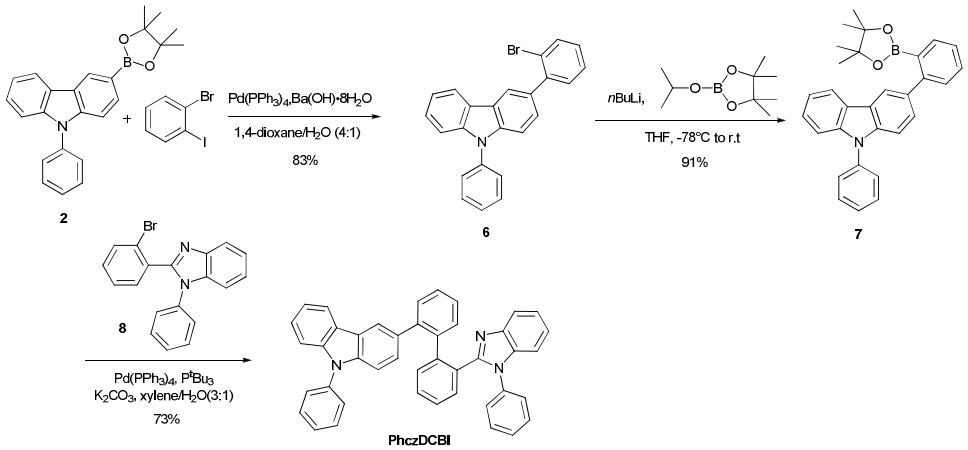

Scheme 1. Synthesis of **PhczCBI, PhczNBI** and **PhczDCBI**.

Crystal Structure

The crystal structures of **PhczNBI** and **PhczCBI** were obtained by x-ray diffraction analysis of their single crystals obtained from a slow evaporation of a CH_2Cl_2: hexanes mixture. Unfortunately, we were unable to grow single crystal for **PhczDCBI**. The relevant crystal data are summarized in Table S1 (ESI).[17] Crystal structures shown in Fig. 1a and 1b demonstrate the *ortho-*/*ortho-* biphenyl spacer successfully imposed highly twisted geometry to the molecules. The dihedral angles between *N*-phenylbenzimidazole/biphenyl linker and carbazole/biphenyl linker were found to be as large as 45.6° and 55.2° for **PhczNBI**, respectively, and 46.2° and 46.3° for **PhczCBI**, respectively. The large dihedral angles between the phenyl rings are beneficial to reducing π-conjugation as well as weakening the electronic interaction between D and A, which are important factors to retain high E_T. In addition, only weak intermolecular π···π stacking was observed in the crystals of **PhczCBI** ($d_{\pi\cdots\pi}$ = 3.5 Å, Fig. 1d). No appreciable dispersive interaction was observed for **PhczNBI**. The lack of intermolecular interactions for **PhczCBI** and **PhczNBI** in the solid states is potential to render an amorphous character with high morphological stability of their

vacuum-deposited films.

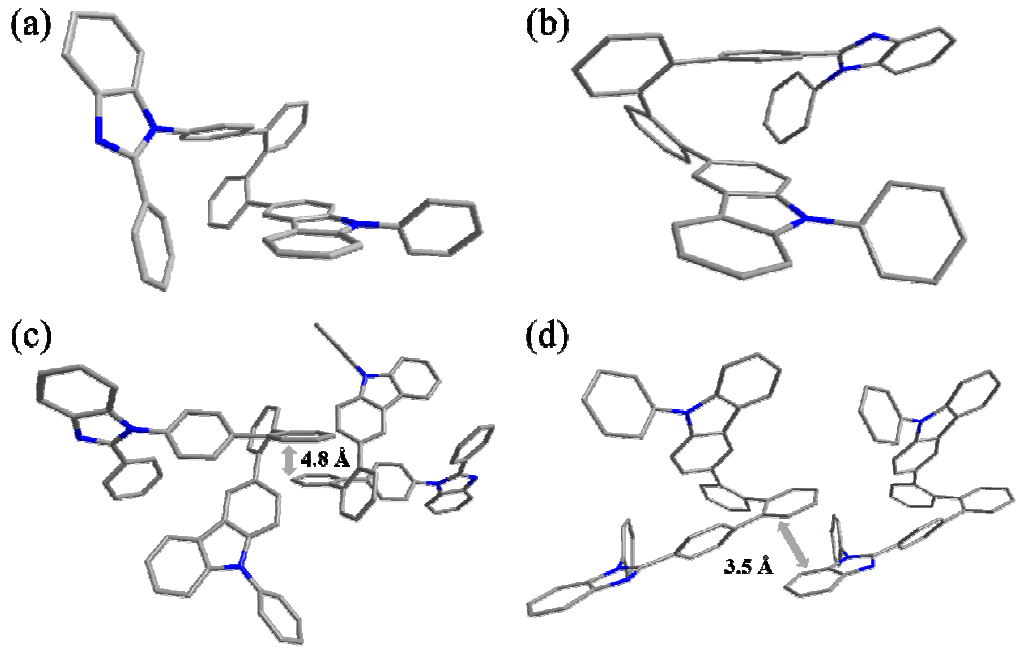

Fig. 1 X-ray structures of (a) **PhczNBI** and (b) **PhczCBI** with their respective intermolecular stacking [(c) and (d)]. The hydrogen atoms are omitted for clarity and thermal ellipsoids are shown at the 50% probability level.

Thermal Properties

Thermogravimetric analysis (TGA) and differential scanning calorimetry (DSC) were used to probe decomposition temperature (T_d, corresponding to 5% weight loss) and glass transition temperature (T_g) under a nitrogen atmosphere for **PhczCBI**, **PhczNBI** and **PhczDCBI** (Table 1). All compounds showed excellent morphological and thermal stabilities in terms of their high T_g and T_d values ranging from 123 to 130 ^oC and 346 to 355 ^oC, respectively. The high T_g and T_d values of these compounds imply that they are capable of enduring not only vacuum thermal sublimation, a general requirement for PhOLED fabrication, but also the inevitable joule heating that

would occur during device operation.

Table 1 Physical properties of **PhczNBI, PhczCBI** and **PhczDCBI**

	$T_g/T_c/T_m$ (°C)	T_d (°C)	E_{ox}/E_{red}[a] (V)	HOMO/LUMO[b] (eV)	HOMO/LUMO $\triangle E_g$[c] (eV)	E_T[d] (eV)	λ_{abs} (nm) Sol./Film	λ_{PL} (nm) Sol./Film	Φ_{PL}[f] Film
PhczNB	124/199/270	346	1.33/-2.10	-5.65/-2.16	-5.82/-2.40 3.42	2.71	290/289	359,375/ 362,383	0.22
PhczCB	130/n.d./n.d.[e]	355	1.28/-2.01	-5.63/-2.28	-5.75/-2.35 3.40	2.55	282/300	420/403	0.67
PhczDCI	123/n.d./n.d.	354	1.32/-2.20	-5.68/-2.10	-5.65/-2.21 3.44	2.70	288/290	357,376/ 364,418	0.15

[a] E_{ox} and E_{red} were estimated from the half-wave and onset potential in the oxidation and reduction scan of the cyclic voltammograms, respectively. [b]Calculated from the electrochemical results with respect to the Fc/Fc^+ redox couple. [c] HOMO was determined using photoelectron yield spectroscopy (AC-2). LUMO = HOMO + E_g, where E_g was calculated from the absorption onset of the solid film. [d] Estimated from onset of the phosphorescence spectra of neat film at 10 K. [e] n.d.: not detected. [f] Photoluminescent quantum efficiency of neat film.

Photophysical Properties

Fig. 2 depicts the UV-vis absorption and photoluminescence (PL) spectra of **PhczNBI**, **PhczCBI**, and **PhczDCBI** recorded at room temperature in CH_2Cl_2 and vacuum-deposited neat films along with their phosphorescence spectra in neat films at 10 K. The data are summarized in Table 1. All compounds exhibited similar absorption profiles in the absorption spectra. We assigned the absorption peaks near 290 nm to the π-π* transition of the *N*-phenylcarbazole moiety whereas the smaller hump near 340 nm is characteristic n-π* transition of carbazole. For PL in solutions, **PhczNBI** and **PhczCBI** exhibited much different emission characteristics. A structured emission spectrum centred at 360 nm was observed for **PhczNBI**, whereas **PhczCBI** showed a red-shifted structureless emission at 420 nm. Apparently, the different emission spectra between **PhczNBI** and **PhczCBI** indicate different

behaviors of their lowest energy excited states. The similar photoluminescent features were also reported in a series of bipolar compounds, in which the structured and structureless emissions were assigned to the emission from locally (Franck-Condon) excited state (LE) and charge transfer state (CT), respectively.[18] Therefore, we attributed the tendency of the lowest excited state whether being located on LE or CT states to the propensity of charge transfer which directly relates to the effectiveness of electronic coupling between D and A in the excited states.[19] Since both **PhczNBI** and **PhczCBI** exhibited highly twisted conformations in solutions as well as in their crystal structures, the charge transfer is less likely to happen by a series of electron hopping through bonds. Therefore, charge transfer process can only occur in a through-space manner when the D and A are close to each other. The crystal structures of **PhczNBI** and **PhczCBI** show that the carbazole and benzimidazole moieties are close to each other in different manners. In **PhczCBI**, the parallel alignment of the D and A planes implies a better configuration with a shorter D-A distance, which benefits the D/A interactions, resulting in the evident CT state emission. The strong CT behaviour of the PL in **PhczCBI** was further verified with evident solvatochromism (Fig. S1), in which the PL emission maximum was red-shifted from 397 nm in toluene to 439 nm in acetonitrile along with a lower PL intensity. In contrast, in addition to the highly twisted conformation, the perpendicular arrangement of the carbazole and benzimidazole moieties found in **PhczNBI** crystals impedes the charge transfer process. Therefore, the lowest excited state of **PhczNBI** is purely a LE state which shows negligible solvent polarity-dependence as shown in Fig. S1. Interestingly, without the extra phenylene linker between the biphenyl bridge and benzimidazole, **PhczDCBI** exhibits an overlapped emission spectrum comprising of a structured emission (~360 nm) and a broad emission centred around 420 nm. The observation of dual emissions from both LE and CT states for **PhczDCBI** is

presumably due to a different molecular conformation, in which the D/A alignment in **PhczDCBI** is speculated to lie at a marginal boundary where the charge transfer is less efficient than that of **PhczCBI** but more efficient than that of **PhczNBI**, resulting in a reversible excited-state two-step reaction (*i.e.*, LE ↔ CT). This result is consistent with the observation of overlapped LE and CT emissions for molecules possessing twisted geometry reported by Ma *et al.*[20] The solvatochromic behaviour of **PhczDCBI** as shown in Fig. S1 also confirms the PL of **PhczDCBI** with combined LE and CT character, in which the LE emission (~360 nm) is not solvent polarity-dependent whereas the CT emission shifts to longer wavelengths with the increase of solvent polarity. In thin films, both **PhczNBI** and **PhczDCBI** showed increased ratios (CT to LE) of their emission components. The increased CT components in solid-state emissions are attributed to the higher charge transfer propensity in the excited state presumably due to shorter intermolecular D-A distances and restricted conformational change in solid states. The photoluminescence quantum yields (Φ_{PL}) of **PhczNBI**, **PhczCBI** and **PhczDCBI** neat films were measured with an integration sphere to be 0.22, 0.67, and 0.15, respectively. Since these new bipolar molecules are designed as host materials for PhOLEDs, from a practical consideration, the phosphorescent spectra of **PhczNBI**, **PhczCBI** and **PhczDCBI** were recorded in neat film at 10 K (Fig. 2) instead of measuring in solution. As depicted in Fig. 1, the phosphorescence of **PhczCBI** is much stronger than those of **PhczNBI** and **PhczDCBI**, the triplet energies (E_T) of **PhczNBI**, **PhczCBI** and **PhczDCBI** were determined to be 2.71, 2.55, and 2.70 eV, respectively, estimated from the onset of the phosphorescence spectra. The E_T values of **PhczCBI**, **PhczNBI** and **PhczDCBI** are sufficiently high to host a wide range of phosphorescent emitters as a result of effective prevention of reverse triplet energy transfer.

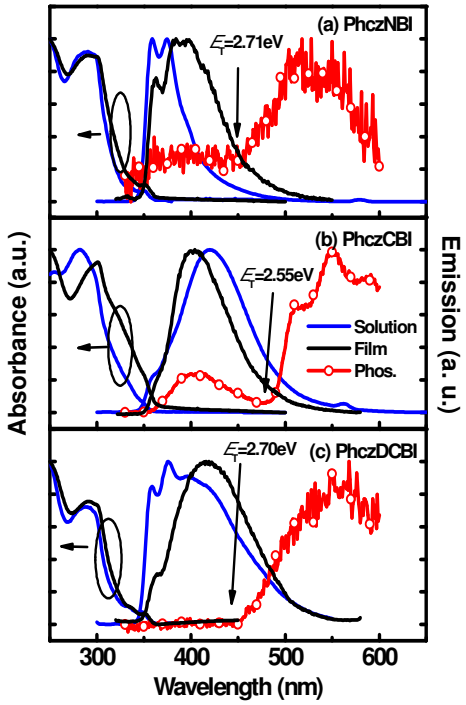

Fig. 2 Room-temperature absorption and emission (PL) spectra of **PhczNBI**, **PhczCBI** and **PhczDCBI** in CH_2Cl_2 solution and in neat films as well as corresponding phosphorescence (Phos) spectra recorded from their neat films at 10 K.

Electrochemical Properties

The electrochemical behaviours of **PhczCBI**, **PhczNBI**, and **PhczDCBI** were investigated by cyclic voltammetry (CV) where tetra(*n*-butyl)ammonium hexafluorophosphate ($TBAPF_6$) in CH_2Cl_2 and tetra(*n*-butyl)ammonium perchlorate (TBAP) in DMF as supporting electrolytes were used for the oxidation and reduction scans, respectively (Fig. 3). Table 1 summarizes the measured redox potentials. All three molecules exhibited one *quasi*-reversible oxidation and an irreversible reduction, arising from their *N*-phenylcarbazole and *N*-phenylbenzimidazole segments, respectively. The new peak appeared at around 1.0 V for the first oxidation scan was due to the dimerization at the C6 position of the carbazole moiety.[21] Obviously, the

reduction onset of **PhczDCBI** is at the highest potential (*ca.* -2.20 V) as compared to those of **PhczNBI** and **PhczCBI**, consistent with the reduced π-conjugation of the benzimidazole moiety due to its highly twisted conformation. Likewise, **PhczNBI** possesses slightly higher redox potentials than those of **PhczCBI** due to the efficient interruption of π-conjugation through N-connection. Refer to the redox of ferrocene/ferrocenium (Fc/Fc^+), the HOMO levels of **PhczCBI**, **PhczNBI**, and **PhczDCBI** can be determined, and the LUMO levels then can be calculated by LUMO = HOMO + E_g, where E_g is the optical energy gap determined from the onset wavelength of the absorption band. The data are summarized in Table 1. However, for the practical applications of **PhczCBI**, **PhczNBI**, and **PhczDCBI** in their solid films, we employed photoelectron yield spectroscopy (Riken AC-2) to determine the HOMO energy levels of **PhczCBI**, **PhczNBI**, and **PhczDCBI** films to be -5.75, -5.82, and -5.65 eV, respectively. The LUMO energy levels were calculated from the HOMO energy levels using the equation of LUMO = HOMO + E_g, where E_g is the optical energy gap determined from the onset wavelength of the film absorption band. The data are summarized in Table 1. Obviously, the HOMO and LUMO energy levels obtained from the solid state are different as compared to those determined from CV presumably due to the complicated intermolecular interactions.

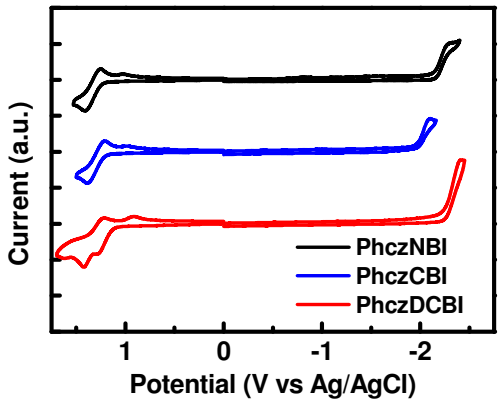

Fig. 3 Cyclic voltammograms of **PhczNBI, PhczCBI** and **PhczDCBI**. Oxidation scan was performed in CH_2Cl_2 with 0.1 M of nBu$_4$NPF$_6$ and reduction scan was performed in DMF with 0.1 M of nBu$_4$NClO$_4$ as a supporting electrolyte. A glassy carbon electrode was used as the working electrode; scan rate 300 mV s^{-1}.

Charge Carrier Mobility

To further understand the charge-carrier transport properties, we used the time-of-flight (TOF) technique[22] to evaluate the carrier mobilities. Representative TOF transients for holes and electrons of **PhczNBI, PhczCBI**, and **PhczDCBI** are shown in Fig. S2. Fig. 4 depicts the obtained carrier mobilities, shown as a function of the square root of the electric field. The hole mobilities varied within the range from 4.4 × 10^{-6} to 7.8 × 10^{-5} cm^2 V^{-1} s^{-1} for fields varying from 3.8 × 10^5 to 1.2 × 10^6 V cm^{-1} and the electron mobilities fell within the range from 6.3 × 10^{-6} to 10^{-4} cm^2 V^{-1} s^{-1} for fields varying from 2.9 × 10^5 to 9 × 10^5 V cm^{-1}. Apparently, *N*-phenylbenzimidazole linking topologies, *i.e.*, C- or N-connection, with the *ortho*-substituted biphenyl linker have crucial influence on the charge transport behavior. Both hole- and electron-mobilities of **PhczNBI** are higher than that of **PhczCBI**. In contrast, the transient photocurrent signals of **PhczDCBI** for electron were too weak for us to evaluate the electron mobility using the TOF technique. To assess the electron transport properties,

we also fabricated electron-only devices having a device structure of ITO/BCP (30 nm)/compounds (50 nm)/TPBI (20 nm)/LiF/Al as shown in Figure 5. Here, low-HOMO 2,9-dimethyl-4,7-diphenyl-1,10-phenanthroline (BCP, μ_e of 10^{-7} cm^2 V^{-1} s^{-1} order)[23] served as the hole-blocking layer to impede the hole carriers in electron-only devices and 1,3,5-tris(*N*-phenylbenzimi-dazol-2-yl)benzene (TPBI, μ_e of 10^{-5} cm^2 V^{-1} s^{-1} order)[24] is used as the electron-transport layer. Excepting enegy barrier in the interface, the magnitude of current density is **PhczNBI** > **PhczCBI** > **PhczDCBI**, which clearly follows the result observed by TOF mobility.

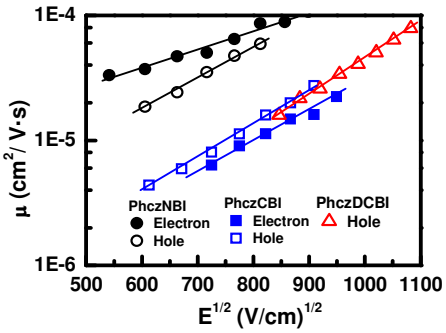

Fig. 4 Electron and hole mobilities versus $E^{1/2}$ for **PhczNBI**, **PhczCBI** and **PhczDCBI**.

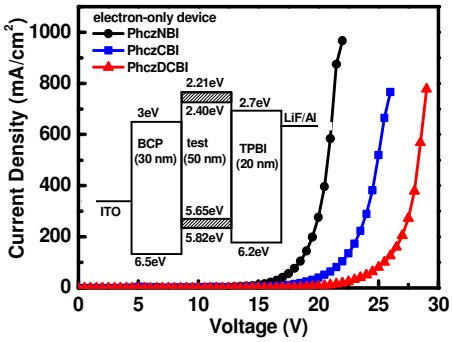

Fig. 5 Current density-voltage (*J*–*V*) characteristics of electron-only devices.

Prior to the device fabrication, photophysical properties of 10 wt% FIrpic-doped host films (100 nm) were evaluated. The transient PL decay curve of FIrpic hosted by

PhczNBI and **PhczDCBI** films exhibited almost a single-exponential decay with a lifetime of 1.31 μs and 1.54 μs, respectively, which indicate the effective confinement of triplet excitons of FIrpic (see ESI in Fig. S3). In contrast, the **PhczCBI**-hosted FIrpic film exhibited a two-component decay, that is, a fast (1.40 μs) decay process and a slow (30 μs) decay process. The latter can be attributed to thermally activated triplet–triplet energy transfer between the host and the guest, such as that in the CBP/FIrpic system (CBP is N,N'-dicarbazolyl-4,4'-biphenyl).[25]

Electroluminescent Properties

To investigate **PhczNBI**, **PhczCBI**, and **PhczDCBI** as bipolar host materials, we fabricated PhOLED devices with three different dopants. We selected iridium(III)[bis(4,6-difluorophenyl)-pyridinato-*N*,$C^{2'}$]picolinate (FIrpic) [26], bis(2-phenylpyridinato)iridium(III) acetylacetonate $[(PPy)_2Ir(acac)]$[1b], and bis(2-phenylbenzothiazolato) (acetylacetonate)iridium(III) $[(Bt)_2Ir(acac)]$[27] as blue, green, and yellow dopants, respectively (Scheme 2). The devices were fabricated with a common structure of ITO/PEDOT:PSS (30 nm)/DTAF (20 nm)/TCTA (5 nm)/host: 10 wt% dopant (25 nm)/DPPS (50nm)/LiF (0.5 nm)/Al (100 nm). To improve the hole injection from the anode, poly(3,4-ethylene-dioxythiophene): poly(styrene sulfonic acid) (PEDOT:PSS) was spun onto the precleaned ITO substrate to form a polymer buffer layer. Two hole-transport layers (HTLs) consisting of a 20-nm-thick layer of 9,9-di[4-(di-*p*-tolyl)aminophenyl]fluorene (DTAF, 20 nm)[28] and a 5-nm-thick layer of 4,4′,4′′-tri(*N*-carbazolyl)triphenylamine (TCTA)[29] were implemented. Next, a 25-nm-thick emissive layer was consisted of 10 wt.% phosphors doped into the host material. To further confine the holes or generated excitons within the emissive layer, a 50-nm-thick diphenylbis[4-(pyridin-3-yl)phenyl]silane (DPPS)[3f] with a high triplet level (E_T: 2.7 eV, HOMO/LUMO: 6.5/2.5 eV) was selected as the electron-transport layer (ETL)

to confine the excitons within the EML. LiF and Al served as the electron-injection layer and cathode, respectively.

Fig. 6-8 depict the current density–voltage–luminance (*J*–*V*–*L*) characteristics, device efficiencies, and EL spectra of the devices. The notation **1**, **2** and **3** indicates the devices fabricated with host materials of **PhczNBI**, **PhczCBI**, and **PhczDCBI**, respectively. FIrpic was incorporated as the blue phosphor to fabricate the blue PhOLEDs named **B1**–**B3**. Analogously, **G1**–**G3**, **Y1**–**Y3**, and **W1**–**W3** were the green, yellow, and white PhOLEDs, respectively. Table 2 summarizes the obtained electroluminescence data. The *J*–*V* characteristics of the devices revealed the electrical properties of the EMLs as a combination of hosts and dopants that influence the charge carrier transport behaviour.

The blue emission device **B1** hosted by **PhczNBI** revealed a maximum brightness (L_{max}) of 21000 cd m^{-2} at 12.5 V (690 mA cm^{-2}) with the CIE coordinates of (0.17, 0.36). The maximum external quantum (η_{ext}), current (η_c), and power efficiencies (η_p) were 12.2%, 24.0 cd A^{-1}, and 20.3 lm W^{-1}, respectively, which are significantly higher than those for **PhczCBI** based device **B2** (4.5%, 9.9 cd A^{-1}, and 7.2 lm W^{-1}) with the CIE coordinates of (0.16, 0.39). Apparently, **PhczCBI** possesses a relatively low triplet energy (E_T = 2.55 eV) that leads to the inefficient confinement of blue excitons, which was verified by the observation of a slow decay process in the transient PL decay characteristics of a FIrpic (10 wt%) doped **PhczCBI** film (Fig. S3). In addition, the EL spectrum (Fig. 7c) of device **B2** displayed a weak emission at ca. 400 nm, which was assigned to the emission from **PhczCBI** due to the highly emissive character (Φ_{PL} = 0.67) and the incomplete energy transfer from **PhczCBI** to FIrpic.

In contrast, **PhczDCBI** with a reduced phenyl linker exhibited the best blue EL performance. Device **B3** based on **PhczDCBI** showed a maximum brightness (L_{max})

of 25800 cd m^{-2} at 14.5 V (680 mA cm^{-2}) and a maximum external quantum efficiency (η_{ext}) of 12.3% corresponding to current efficiency (η_c) of 24.5 cd A^{-1} and power efficiency (η_p) of 20.6 lm W^{-1} with CIE coordinates of (0.15, 0.33). At a high brightness of 1000 cd m^{-2}, the η_{ext} of devices **B1** and **B3** are still as high as 7.9% and 11.6%, respectively, showing low efficiency roll-off (Table 2). However, the blue device performances are moderate among FIrpic-based OLEDs presumably because the E_Ts of **PhczNBI** (2.70 eV) and **PhczDCBI** (2.71 eV) are not sufficiently high for blocking the thermal activated exciton diffusion process. To further verify the energy transfer behaviour of host, Φ_{PL} characteristics of films with FIrpic (10 wt%) doped in **PhczNBI**, **PhczDCBI** and mCP were investigated under a N_2 flow using an integrating sphere equipped with a multichannel spectrometer as the optical detector (see ESI in Table S2). The Φ_{PL} of FIrpic/mCP film is 0.95, which is higher than those of **PhczNBI** (0.71)- and **PhczDCBI** (0.73) hosted films (see ESI in Table S2). The η_{ext} of the device **B3** was similar with that of the device **B1**, which is consistent with the observation of Φ_{PL}.

To further evaluate the suitability of these new compounds as host materials for low energy triplet emitters, we also tried to evaluate green and yellow PhOLEDs using phosphorescent dopants $(PPy)_2Ir(acac)$ and $(Bt)_2Ir(acac)$, respectively. These devices achieved better performances as compared to those of blue devices (Table 2). All devices exhibited high performance with a rather low efficiency roll-off at high brightness. For instance, green device **G2** with **PhczCBI** as the host achieved a L_{max} of 158600 cd m^{-2} at 14 V and respectable EL efficiencies (18.7%, 69.2 cd A^{-1}, and 66.3 lm W^{-1}) with η_{ext} of 17.9% at brightness of 1000 cd m^{-2}; while yellow device **Y1** with **PhczNBI** as the host achieved a L_{max} of 121700 cd m^{-2} at 15 V and respectable EL efficiencies (19.6%, 51 cd A^{-1}, and 43.1 lm W^{-1}) with η_{ext} of 18.7% at brightness of 1000 cd m^{-2}. The remarkably reduced efficiency roll-off is the combined results of

the characteristics of the hosts and the suitable device configuration, which lead to a balanced carrier injection and transport in EMLs as well as facilitate a uniform distribution of carriers and excitons to reduce the field-assisted exciton dissociation.[9,10,30] All devices (except for device B2 hosted by **PhczCBI**) displayed relatively pure emission from blue to red as shown in Fig. 6c–8c, indicating that the electroluminescence can be completely confined on the emissive dopants.

We also fabricated two-emitter white OLEDs (WOLEDs) (device **W1**–**W3**) utilizing 10 wt% FIrpic and 0.2–1 wt% $(Bt)_2Ir(acac)$ co-doped into the hosts as a single emitting layer. The proportion of $(Bt)_2Ir(acac)$ required to produce balanced white emission in these devices was relatively low because the yellow emission is either from efficient energy transfer of the blue phosphor or direct exciton formation through charge-trapping on the yellow dopant. Device **W3** hosted by **PhczDCBI** exhibited the best performance, which achieved a L_{max} of 57100 cd m^{-2} at 13.5 V and respectable EL efficiencies (13.9%, 34.9 cd A^{-1}, and 24.8 lm W^{-1}). The efficiencies of device **W3** were higher than those of the device **W1** and **W2** because of a higher ratio of blue emission in device **W3**. All WOLEDs exhibited a voltage-dependent EL spectrum. As the operation voltage increased, the relative intensity of blue emission increased, led to a slight shift of the CIE coordinates. For example, when the voltage increases from 7 to 11 V, the CIE coordinates slightly vary from (0.37, 0.43) to (0.34, 0.42) for device **W3**, and the color-rendering indices (CRI) was shifted from 64.8 to 65.5. This is due to the low concentration of $(Bt)_2Ir(acac)$ in the blend which results in

the partial saturation of emission from $(Bt)_2Ir(acac)$ and the easier formation of blue emission at higher voltages.[31]

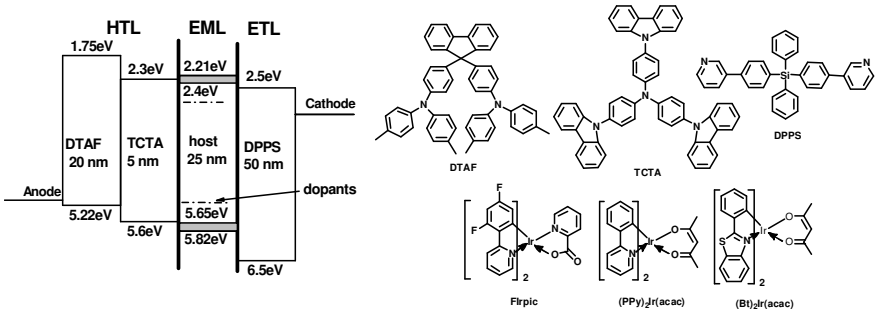

Scheme 2 Molecular structures used in this study and an energy level diagram of the device.

Table 2 EL performance of devices incorporating various hosts and emitter

	Host: 10% dopant	V_{on}[a] [V]	at 1000 nit [V,%]	L_{max} [cd m^{-2}]	I_{max} [mA cm^{-2}]	η_{ext} [%]	η_c [cd A^{-1}]	η_p [lm W^{-1}]	CIE [x,y]
B1	PhczNBI: FIrpic	3.0	7, 10.0	21000 (12.5V)	690	12.2	24.0	20.3	0.17,0.36
G1	PhczNBI: $PPy_2Iracac$	2.5	6, 16.1	104300 (14.5V)	690	16.1	58.1	48.4	0.33,0.63
Y1	PhczNBI: $Bt_2Iracac$	2.5	6.6, 18.7	121700 (15 V)	810	19.6	51	43.1	0.52,0.47
W1	PhczNBI: 10%FIrpic: 0.3% $Bt_2Iracac$ %	3.0	7, 13.2	34800 (14.5V)	650	13.4	33.4	21	0.35,0.43
B2	PhczCBI: FIrpic	3.0	10, 1.8	5700 (15V)	720	4.5	9.9	7.2	0.16,0.39
G2	PhczCBI: $PPy_2Iracac$	2.5	6, 17.9	158600 (14V)	970	18.7	69.2	66.3	0.33, 0.62
Y2	PhczCBI: $Bt_2Iracac$	2.5	5.8, 17.5	131900 (13.5 V)	1000	18.7	47	42.2	0.52,0.47
W2	PhczCBI: 10%FIrpic: 0.2% $Bt_2Iracac$ %	3.0	9, 5	11500 (15.5V)	730	7.7	19.8	12.6	0.34,0.45
B3	PhczDCBI: FIrpic	3.0	8.2, 11.6	25800 (14.5V)	680	12.3	24.5	20.6	0.15,0.33
G3	PhczDCBI: $PPy_2Iracac$	2.5	6, 15.0	166000 (13.5V)	990	15.1	54.6	43.2	0.33, 0.62
Y3	PhczDCBI: $Bt_2Iracac$	2.5	6.5, 15.7	100200 (14.5 V)	920	16.1	42.6	34.9	0.52,0.48
W3	PhczDCBI: 10%FIrpic: 1% $Bt_2Iracac$ %	2.5	6.8, 13.8	57100 (13.5V)	860	13.9	34.9	24.8	0.36,0.43

[a] Turn-on voltage at which emission became detectable (10^{-2} cd m^{-2}). The notation 1, 2 and 3 indicate the devices fabricated with host materials of **PhczNBI**, **PhczCBI**, and **PhczDCBI**, respectively, in the configuration: ITO/PEDOT:PSS/DTAF (20nm)/TCTA (5 nm)/emitter (25 nm)/DPPS (50nm)/LiF/Al.

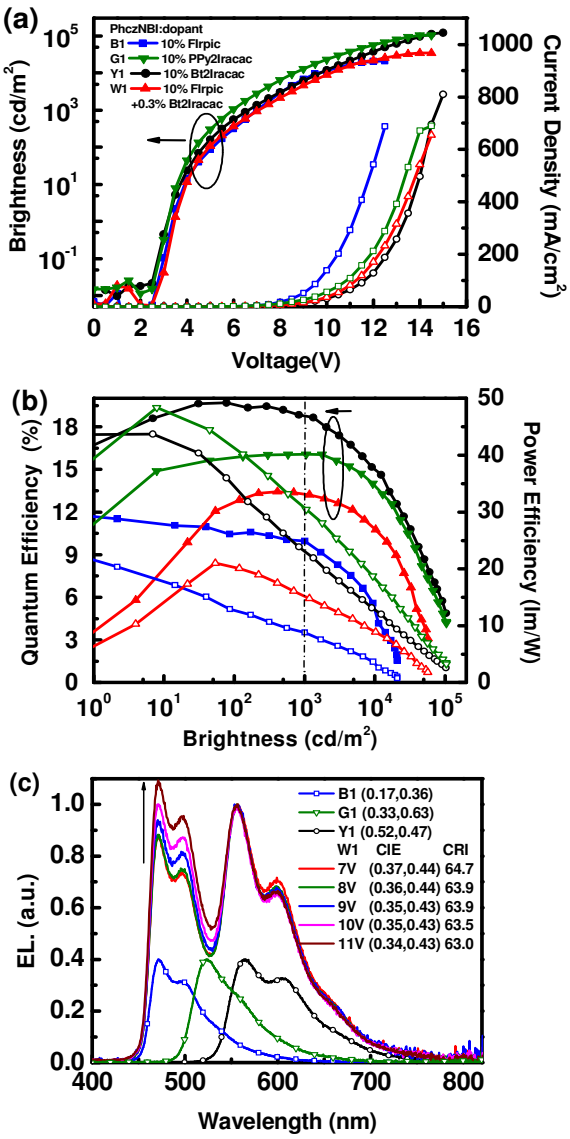

Fig. 6 (a) Current density-voltage-luminance (*J*–*V*–*L*) characteristics. (b) External quantum (η_{ext}) and power efficiencies (η_P) as a function of brightness. (c) EL spectra of **PhczNBI**-based devices.

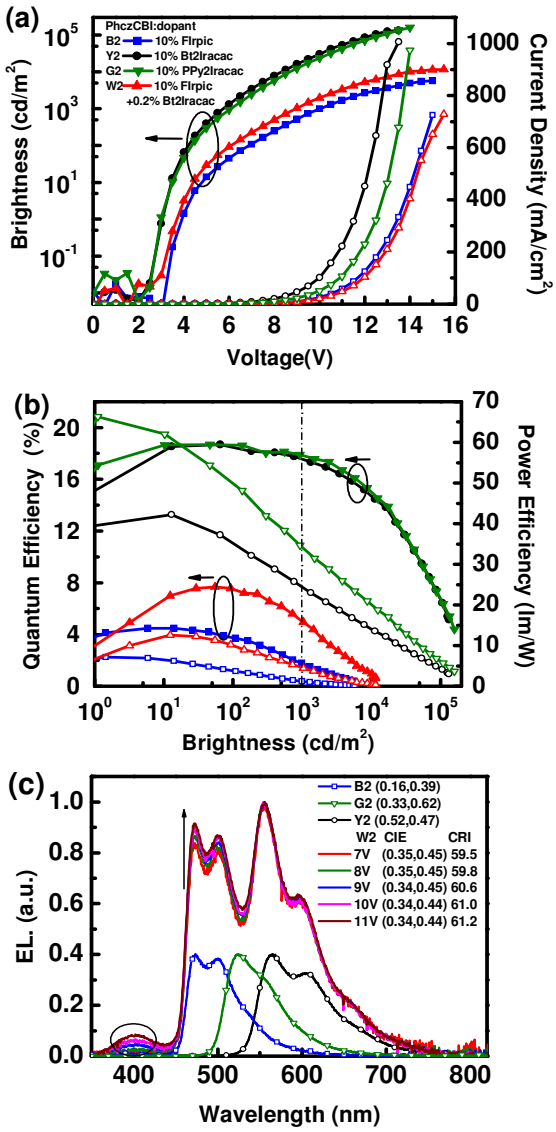

Fig. 7 (a) Current density-voltage-luminance (*J*–*V*–*L*) characteristics. (b) External quantum (η_{ext}) and power efficiencies (η_P) as a function of brightness. (c) EL spectra of **PhczCBI**-based devices.

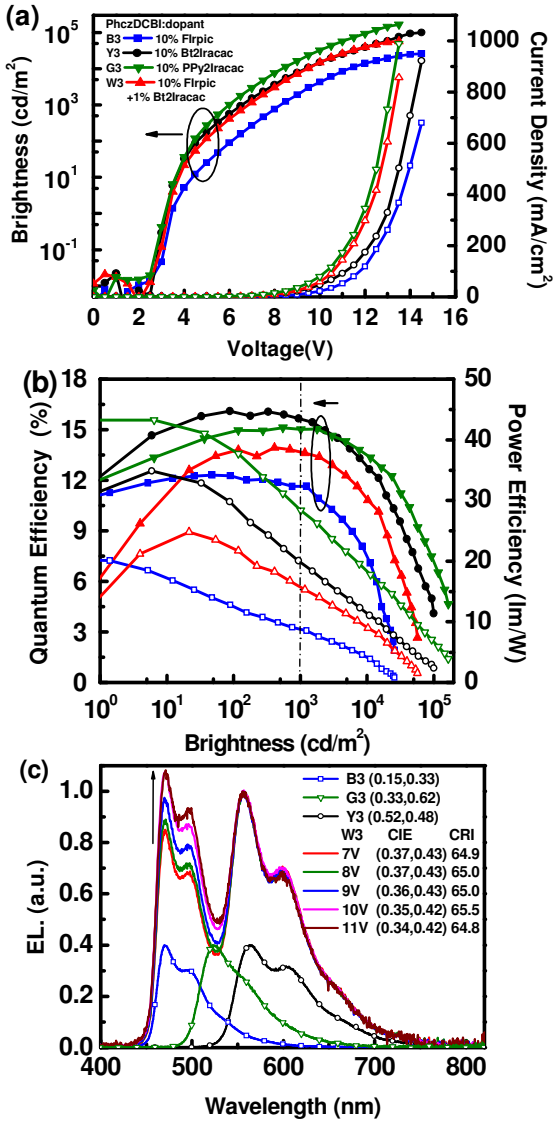

Fig. 8 (a) Current density-voltage-luminance (*J*–*V*–*L*) characteristics. (b) External quantum (η_{ext}) and power efficiencies (η_P) as a function of brightness. (c) EL spectra of **PhczDCBI**-based devices.

Conclusion

We have successfully designed and synthesized three bipolar host materials **PhczNBI**, **PhczCBI**, and **PhczDCBI**, in which the donor 9-phenylcarbazole and the acceptor benzimidazole were bridged through a 2,2'-biphenyl linker. The *ortho-ortho* linkage imparts these bipolar hosts highly twisted molecular conformations which not only benefit to the morphological stability but also endow sufficiently high triplet levels for hosting a wide range of phosphorescent dopants. Different linking topologies (*C*- or *N*-connectivity) between the benzimidazole group and the biphenyl linker resulted in different effective π-conjugation and different E_T. All three bipolar hosts exhibited high morphological and thermal stability as well as balanced carrier transport characteristics. Consequently, highly efficient blue, green, yellow, and white PhOLEDs based on these host materials were fabricated. Among the three host materials, **PhczDCBI** as the host gave the highest device efficiencies for blue- and white-emitting devices (12.3%, 24.5 cd A^{-1}, 20.6 lm W^{-1} for device **B3** and 13.9%, 34.9 cd A^{-1}, and 24.8 lm W^{-1} for device **W3**, respectively) with low efficiency roll-off. We believe that the molecular design approach reported in this work with tailored donor/acceptor and bridge moieties can lead to suitable host materials, rendering high efficiency PhOLEDs feasible.

Acknowledgements

This study was supported financially by the National Science Council of Taiwan (NSC 100-2112-M-019-002-MY3, 101-2113-M-002-009-MY3).

References

[1] (a) M. A. Baldo, D. F. O'Brien, Y. You, A. Shoustikov, S. Sibley, M. E. Thompson and S. R. Forrest, *Nature*, 1998, **395**, 151; (b) C. Adachi, M. A. Baldo, M. E. Thompson and S. R. Forrest, *J. Appl. Phys.*, 2001, **90**, 5048; (c) S. Reineke, F. Lindner, G. Schwartz, N. Seidler, K. Walzer, B. Lüssem and K. Leo, *Nature*, 2009, **459**, 234; (d) C.-H. Chang, H.-C. Cheng, Y.-J. Lu, K.-C. Tien, H.-W. Lin, C.-L. Lin, C.-J. Yang and C.-C. Wu, *Org. Electron*., 2010, **11**, 247; (e) C.-H. Chang, K.-C. Tien, C.-C. Chen, M.-S. Lin, H.-C. Cheng, S.-H. Liu, C.-C. Wu, J.-Y. Hung, Y.-C. Chiu and Y. Chi, *Org. Electron.*, 2010, **11**, 412.

[2] (a) H. Yersin, W. J. Finkenzeller, in *Highly Efficient OLEDs with Phosphorescent Materials*, ed. H. Yersin, Wiley-VCH, Weinheim, 2008, ch. 1; (b) J. Kalinowski, in *Organic Electroluminescence*, ed. Z. H. Kafafi, Taylor & Francis Group, CRC Press, Boca Raton, 2005, ch. 2.

[3] (a) A. Köhler, J. S. Wilson and R. H. Friend, *Adv. Mater.*, 2002, **14**, 701; (b) W. S. Huang, J. T. Lin, C. H. Chien, Y. T. Tao, S. S. Sun and Y. S. Wen, *Chem. Mater.*, 2004, **16**, 2480; (c) J. Ding, J. Gao, Y. Cheng, Z. Xie, L. Wang, D. Ma, X. Jing and F. Wang, *Adv. Funct. Mater.*, 2006, **16**, 575; (d) T. Tsuzuki and S. Tokito, *Adv. Mater.*, 2007, **19**, 276; (e) E. Orselli, R. Q. Albuquerque, P. M. Fransen, R. Fröhlich, H. M. Janssen and L. D. Cola, *J. Mater. Chem.*, 2008, **18**, 4579; (f) L. Xiao, S.-J. Su, Y. Agata, H. Lan and J. Kido, *Adv. Mater.*, 2009, **21**, 1271.

[4] C. Murawski, K. Leo and M. C. Gather, *Adv. Mater.*, 2013, **25**, 6801.

[5] M. Sudhakar, P. I. Djurovich, T. E. Hogen-Esch and M. E. Thompson, *J. Am. Chem. Soc.,* 2003, **125**, 7796.

[6] (a) J. S. Swensen, E. Polikarpov, A. V. Ruden, L. Wang, L. S. Sapochak and A. B. Padmaperuma, *Adv. Mater.*, 2011, **21**, 3250; (b) K. Goushi, R. Kwong, J. J. Brown, H. Sasabe and C. Adachi, *J. Appl. Phys.*, 2004, **95**, 7798.

[7] Y. Tao, C. Yang and J. Qin, *Chem. Soc. Rev.*, 2011, **40**, 2943.

[8] (a) R. Guo, D. Hu, S. Yue, Z. Zhang, Y. Duan, P. Lu, Y. Ma, Y. Zhao and S. Liu, *J. Phys. D: Appl. Phys.*, 2013, **46**, 265101; (b) H.-F. Chen, T.-C. Wang, W.-Y. Hung, H.-C. Chiu, C. Yun and K.-T. Wong, *J. Mater. Chem.*, 2012, **22**, 9658; (c) Y. J. Cho and J. Y. Lee, *J. Phys. Chem. C*, 2011, **115**, 10272; (d) A. Chaskar, H.-F. Chen and K.-T. Wong, *Adv. Mater.*, 2011, **23**, 3876.

[9] S. Gong, Y. Chen, C. Yang, C. Zhong, J. Qin and D. Ma, *Adv. Mater.,* 2010, **22**, 5370.

[10] S. Gong, Y. Chen, J. Luo, C. Yang, C. Zhong, J. Qin and D. Ma, *Adv. Funct. Mater.,* 2011, **21**, 1168.

[11] (a) S.-Y. Ku, W.-Y. Hung, C.-W. Chen, S.-W. Yang, E. Mondal, Y. Chi and K.-T. Wong, *Chem. Asian J.,* 2012, **7**, 133; (b) W.-Y. Hung, T.-C. Wang, H.-C. Chiu, H.-F. Chen and K.-T. Wong, *Phys. Chem. Chem. Phys.*, 2010, **12**, 10685; (c) F.-M. Hsu, C.-H. Chien, Y.-J. Hsieh, C.-H. Wu, C.-F. Shu, S.-W. Liu and C.-T. Chen, *J. Mater. Chem.*, 2009, **19**, 8002.

[12] E. Mondal, W.-Y. Hung, H.-C. Dai and K.-T. Wong, *Adv. Funct. Mater.*, 2013, **23**, 3096.

[13] C. Fan, F. Zhao, P. Gan, S. Yang, T. Liu, C. Zhong, D. Ma, J. Qin and C. Yang, *Chem. Eur. J.,* 2012, **18**, 5510.

[14] (a) B. Pan, B. Wang, Y. Wang, P. Xu, L. Wang, J. Chen and D. Ma, *J. Mater. Chem. C*, 2014, **2**, 2466; (b) S.-H. Chou, W.-Y. Hung, C.-M. Chen, Q.-Y. Liu, Y.-H. Liu and K.-T. Wong, *RSC Adv*., 2013, **3**, 13891; (c) H.-C. Ting, Y.-M. Chen, H.-W. You, W.-Y. Hung, S.-H. Lin, A. Chaskar, S.-H. Chou, Y. Chi, R.-H. Liu and K.-T. Wong, *J. Mater. Chem*., 2012, **22**, 8399; (d) J. H. Park, E. K. Kim, I. M. El-Deeb, S. J. Jung, D. H. Choi, D.-H. Kim, K. H. Yoo, J. H. Kwon and S. H. Lee, *Bull. Korean Chem. Soc.*, 2011, **32**, 841; (e) D. Thirion, J. Rault-Berthelot, L. Vignau and C. Poriel, *Org. Lett.*, 2011, **13**, 4418; (f) M.-Y. Lai, C.-H. Chen, W.-S. Huang, J. T. Lin, T.-H. Ke, L.-Y. Chen, M.-H. Tsai and C.-C. Wu, *Angew. Chem. Int. Ed.*, 2008, **47**, 581.

[15] Y.-M. Chen, W.-Y. Hung, H.-W. You, A. Chaskar, H.-C. Ting, H.-F. Chen, K.-T. Wong and Y.-H. Liu, *J. Mater. Chem.*, 2011, **21**, 14971.

[16] F. R. Leroux, L. Bonnafoux, C. Heiss, F. Colobert and D. A. Lanfranchi *Adv. Synth. Catal.,* 2007, **349**, 2705.

[17] The crystallographic data (excluding structure factors) have been deposited at the Cambridge Crystallographic Data Centre and allocated the deposition numbers CCDC 1007528 and 1007529 for **PhczNBI** and **PhczCBI**, respectively. These data can be obtained free of charge from The Cambridge Crystallographic Data Centre *via* www.ccdc.cam.ac.uk/data_request/cif.

[18] (a) A. Baschieri, L. Sambri, I. Gualandi, D. Tonelli, F. Monti, A. D. Esposti and N. Armaroli, *RSC Adv*., 2013, **3**, 6507; (b) V. A. Galievsky, S. I. Druzhinin, A. Demeter, P. Mayer, S. A. Kovalenko, T. A. Senyushkina and K. A. Zachariasse, *J. Phys. Chem. A*, 2010, **114**, 12622; (b) A. W. Grabowski, K. Rotkiewicz and W. Rettig, *Chem. Rev.*, 2003, **103**, 3899.

[19] G. Ramunni and L. Salem, *Zeitschrift für Physikalische Chemie*, 1976, **101**, 123.

[20] W. Li, D. Liu, F. Shen, D. Ma, Z. Wang, T. Feng, Y. Xu, B. Yang and Y. Ma, *Adv. Funct. Mater.*, 2012, **22**, 2797.

[21] (a) K. E. Linton, A. L. Fisher, C. Pearson, M. A. Fox, L.-O.Pålsson, M. R. Bryce, and M. C. Petty, *J. Mater. Chem.*, 2012, **22**, 11816; (b) J. He, H. Liu, Y. Dai, X. Ou, J. Wang, S. Tao, X. Zhang, P. Wang and D. Ma, *J. Phys. Chem. C*, 2009, **113**, 6761; (c) M. Sonntag and P. Strohriegl, *Chem. Mater.*, 2004, **16**, 4736; (d) G. Zotti, G. Schiavon, S. Zecchin, J.-F.Morin and M. Leclerc, *Macromolecules*, 2002, **35**, 2122.

[22] P. M. Borsenberger and D. S. Weiss, in *Organic Photoreceptors for Imaging Systems*, Marcel Dekker, New York, 1993.

[23] Z.-Y. Xie, T.-C. Wong, L.-S. Hung and S.-T. Lee, *Appl. Phys. Lett*., 2002, **80**, 1477.

[24] W.-Y. Hung, T.-H. Ke, Y.-T. Lin, C.-C. Wu, T.-H. Hung, T.-C. Chao, K.-T. Wong and C.-I. Wu, *Appl. Phys. Lett.,* 2006, **88**, 064102.

[25] S. Tokito, T. Iijima, Y. Suzuri, H. Kita, T. Tsuzuki and F. Sato, *Appl. Phys. Lett.*, 2003, **83**, 569.

[26] R. J. Holmes, S. R. Forrest, Y.-J. Tung, R. C. Kwong, J. J. Brown, S. Garon and M. E. Thompson, *Appl. Phys. Lett.*, 2003, **82**, 2422.

[27] S. Lamansky, P. Djurovich, D. Murphy, F. Abdel-Razzaq, H.-E. Lee, C. Adachi, P. E. Burrows, S. R. Forrest and M. E. Thompson, *J. Am. Chem. Soc.*, 2001, **123**, 4304.

[28] M.-T. Kao, W.-Y. Hung, Z.-H. Tsai, H.-W. You, H.-F. Chen, Y. Chi and K.-T. Wong, *J. Mater. Chem.*, 2011, **21**, 1846.

[29] (a) S.-J. Su, E. Gonmori, H. Sasabe and J. Kido, *Adv. Mater.*, 2008, **20**, 4189; (b) Y.-Y. Lyu, J. Kwak, W. S. Jeon, Y. Byun, H. S. Lee, D. Kim, C. Lee and K. Char, *Adv. Funct. Mater.,* 2009, **19**, 420.

[30] Q. Wang, J. Ding, D. Ma, Y. Cheng, L. Wang and F. Wang, *Adv*. *Mater*., 2009, **21**,

2397.

[31] (a) Y. Shao and Y. Yang, *Appl. Phys. Lett.*, 2005, **86**, 073510; (b) J. Huang, G. Li, E. Wu, Q. Xu and Y. Yang, *Adv. Mater.,* 2006, **18**, 114; (c) Q. Wang, J. Ding, D. Ma, Y. Cheng, L. Wang, X. Jing and F. Wang, *Adv. Funct. Mater.,* 2009, **19**, 84.